High-resolution ellipsometric studies on fluid interfaces

Antonio Stocco, Klaus Tauer

EPJ manuscript No.
(will be inserted by the editor)

High resolution ellipsometric studies on fluid interfaces

Antonio Stocco[1,2,a], Klaus Tauer[1]

[1] Max Planck Institute of Colloids and Interfaces, 14476 Golm, Germany
[2] Laboratoire de Physique des Solides, University Paris-Sud, F-91405 Orsay Cedex, France

Abstract. In this article, highly accurate experimental results reveal the interfacial profile between different macroscopic fluid phases. The deviation from a step profile, quantified by the ellipsometric quantity J_1, shows a strong correlation with the cohesive energy quantified by the Gordon parameter G. Surprisingly, at high values of G, $J_1(< 0)$ deviates significantly from any predictions. Findings for water and water-like interfaces can be interpreted in terms of the strength of hydrogen bonding at the surface.

1 Introduction

A liquid interface is a stage where intermolecular forces show their strength and their specific properties. Different types of molecular interactions cause interface tensions of varying strength and also affect the density profile perpendicular to the interface. Hence, the interface between two fluids is never infinitely sharp [1]. Density gradients on either side of the interface cause several unexpected but interesting effects. For instance, experimental evidence has been given recently that spontaneous droplet formation occurs which is assumed to be due to local supersaturation in interfacial layers [2]. This example shows that a molecular understanding of the apparently simple case of an interface between two pure liquids is still lacking. Probably, different experimental investigation of interfaces will evidence further unexpected results which in turn may need interpretation out of the box of established thinking.

The simplest case is an apolar liquid, where interactions are caused exclusively by dispersion forces. Here, already a simple model based on packing arguments and macroscopic solvent properties (bulk density, boiling temperature or heat of evaporation as a measure of cohesive energy) is able to reproduce quite accurately experimental values for the interface tension [3]. Slightly more complicated are polar solvents, where also dipolar interactions contribute and possibly create an orientation of molecules at the interface. Such an orientation at an interface is also observed for nematic liquid crystals in the isotropic phase (see e. g. [4]). In this case, steric repulsion and anisotropy of dispersion forces create the local orientation as a cooperative effect induced by the interface. Most complicated and most specific are interactions via hydrogen bonds with highly directional character. The most famous and studied example is water, which already presents anomalies in the bulk phase and peculiar elastic and viscous properties at the interfacial region [5].
The description of such transition region is of great importance in many scientific and industrial fields such as transport phenomena, separation processes including complex fluids and biology. On different length scales, the interfacial region can be described either by a smooth density or concentration profile, or by surface waves, i. e. capillary waves [6]. Within the first approach several theoretical expressions were developed [7], whereas in the capillary wave theory the sur-

[a] e-mail: stocco@lps.u-psud.fr

face roughness defines the width of the interface [8]. In both cases the density of the interfacial region changes monotonously and the average density of the interfacial region is expected in between the density values of the two macroscopic bulk phases.
A well established technique for the investigation of an interfacial profile is ellipsometry. In ellipsometry, the imaginary part of the ratio between the reflective coefficient in p and s polarization, $\mathrm{Im}(r_p/r_s)=\bar{\rho}$, is used to describe the interfacial profile at the principal angle where $\mathrm{Re}(r_p/r_s)=0$. Note that the latter angle gives an operative definition of the Brewster angle $\varphi_B = \arctan(n_2/n_1)$, where n_1 and n_2 are the refractive index of the medium 1 and 2 respectively [9,10].
When the light travels first in the lower refractive index media, $\bar{\rho}$ is predicted by the previous theories to be positive. Meunier studied critical interfaces and several liquid/air interfaces [11]. The experimental ellipticity $\bar{\rho}$ reported were always positive according to the prediction but significant deviation from the absolute values were also found. In the case of air/water a 40% discrepancy between the experimental and the theoretical value, calculated with coupled capillary waves and no surface rigidity, was found.

However, few exceptions for negative $\bar{\rho}$ were also reported. This was for instance the case of the first measurements on water performed by Jamin in 1851 [12] and by Beaglehole in 1987, who found an interfacial density of water above the bulk value during heating cycles [13]. On the other hand, a depleted layer was extensively postulated for the interpretation of the water/liquid or water/solid interfacial profiles measured by x-ray [14,15].

Theoretically, an increase or a deficit in water density is predicted as a function of the size of an apolar solute [16] as a consequence of the hydrophobic effect [17]. In simulation studies, the water molecule is usually geometrically modeled with three arms, representing the hydrogen bonds, forming a 2D disk (Mercedes Benz model). Within the latter model, it is predicted that the water molecule, in contact with a planar apolar phase, points one of its hydrogen towards the surface, loosing one hydrogen bond [17].
Sum frequency vibrational spectroscopy studies confirmed the latter theoretical prediction. The structure of water molecules at the air/water interface, in fact, is more ordered than in the bulk phase being the spectrum similar to ice water. Nonetheless the structure of those molecules is less order than ice water with a OH dangling bond at the surface every four molecules [18]. Thus, the surface of water is composed by a hydrogen-bonding network such as the hexagonal ice structure but partially disordered or distorted.
Ice/water interfaces were studied by ellipsometry by Beaglehole and Wilson. For these interfaces, they reported negative values of the ellipsometric J_1 (see Eq. 3) and interpreted their results in terms of interfacial anisotropy [19]. For ice , the refractive index parallel and perpendicular to the interface (in the basal plane) are $n_{\parallel}$=1.309 and $n_{\perp}$=1.307 respectively. Anisotropy of bond polarizability was also detected by Raman spectroscopy and light scattering for water vapor [20]. Computer simulations on water/vacuum and water/hydrophobic media pointed out that the total polarization of water molecules increases close to the interface [21,22]. Similarly, Kudin and Car to explain the charging of water/hydrophobic interface predicted a amphiphilic behavior for both H^+ and OH^- at the interface [23].
Water molecules in confined geometries behave differently also from a dynamic viewpoint. The translational diffusion is not suppressed when water is confined between two solid walls despite an increasing density due to the lost of hydrogen bonds is discussed [24]. Like volumetric anomaly observed in the bulk phase under cooling, the effect of confinement between two solid planes or in pores seems to be related to the attractive interactions exerted in the confined system [25]. However, those scenarios are depicted for water between two solid interfaces whereas this work focuses on the interface between two macroscopic fluids.
In the recent years, new impulses for an understanding of the phenomena that take place at the surface of a liquid were given also experimentally either by means of new observations [26,27] or new techniques, e.g. x-ray synchrotron surface scattering [28].
In this paper we reported ellipsometric data of several air/liquid interfaces and a water/dodecane interface, discussing our new findings together with theories and experiments.

2 Experimental Section

Double distilled and deionized water W from a Milli-Q-RG ultrafiltration system, decane DE (Aldrich, $\geq$ 99.8 %), dodecane DD (Aldrich, $\geq$ 99.8 %), formic acid F (Aldrich, $\geq$ 98 %), 1-Methyl-2-pyrrolidone (NMP) N (Aldrich, $\geq$ 99.5 %), hydrazine monohydrate H (Aldrich, $\geq$ 98 %) were used. Samples were filtered twice through a 0.2 μm Teflon membrane (Millipore).

The interfaces were cleaned several times by sucking the top layers in order to remove bubbles, dust and impurities.

Between every cleaning step 1 hour was waited in order to reequilibrate the system and align the interfacial level. At least two samples of each system were prepared in each case at least three ellipsometric scans were performed at different times after preparation, ranging from 4 to 24 hour.

Reflection ellipsometry was performed on a home built apparatus [29] working with a 25mW HeNe-laser (wavelength $\lambda = 633$ nm). An open deep dish of 8 cm diameter was used as sample holder. Alternately, a cylindrical glass cell of large enough size (7.5 cm diameter and 7.5 cm length) in order to minimize the surface curvature due to meniscus effects is filled up to half the volume, so the center of rotation of the cylinder lies within the interface. This geometry allows reflection measurements from above the interface through air or from below the interface, through the liquid. Except for the water/dodecane and water/air interface (measurements performed from the water side), all measurements in this work were performed from above (from the air side). In this article, we labeled the interfaces describing first the media in which the incident light travels; e.g. air/water (A/W) and water/dodecane (W/DD). The apparatus is placed on an active vibration table (HWL, Ammerbuch, Germany) to provide an isolation from external perturbations.

For high accuracy, a multiple angle of incidence (φ is the angle of incidence) and nulling scheme developed for ellipsometric light scattering (ELS) [30,31,32] has been adopted for reflection ellipsometry. It relies on a two dimensional scan of polarizer and analyzer and a suitable two dimensional fit [33]. The complex ellipsometric coefficientρ equal to the ratio of the reflectivities r_p and r_s is related to the two real ellipsometric parameters Ψ and Δ: [9]

$$\rho = \frac{r_p}{r_s} = \tan(\Psi) \cdot \exp(i\Delta). \tag{1}$$

For rough interfaces as e. g. created by capillary waves, nulling-ellipsometry detects the coherent signal which represents the averaged refractive index profile of the interface [34]. The connection of r_s and r_p with Ψ and Δ in this case is slightly modified, however, close to the Brewster angle where investigations in this work have been performed Eq. 1 remains a good approximation.

Data are analyzed in the framework of a Perturbation theory [10], which describes the deviation of the complex ellipsometric coefficient from the the ratio of the reflectivities $r_{p,0}/r_{s,0}$ for a sharp step-like profile:

$$\frac{r_p}{r_s} = \frac{r_{p,0}}{r_{s,0}} - \frac{2iQ_1}{r_{s,0}(Q_1+Q_2)^2}\frac{K^2}{n_1^2 n_2^2} J_1. \tag{2}$$

Here, $Q_i = 2\pi/(n_i\lambda)\cdot\cos\varphi_i$ (Snell's law $n_1 \sin\varphi_1 = n_2 \sin\varphi_2$ relates φ_1 to φ_2), $K = 2\pi n_1/\lambda\cdot\sin\varphi_1$ and the first order invariant:

$$J_1 = \int_{-\infty}^{+\infty} \frac{(n_1^2 - n_m^2)(n_m^2 - n_2^2)}{n_m^2}\, \mathrm{d}z, \tag{3}$$

combines the extension and the optical contrast of the transition zone in a single parameter. It is not possible to determine the extension and the optical contrast separately for thin interfacial layers. The refractive index profile $n_m(z)$ along the coordinate z normal to the interface adopts the limiting bulk values n_1 and n_2 in the top and the bottom medium, respectively. Only the interface region contributes to the the integration in equation 3.

A positive value of J_1 is characteristic of an interface layer with a refractive index n_m in between the value of the two macroscopic phases ($n_1 < n_m < n_2$). Whereas $J_1 < 0$ refers to the case

where the value of n_m is not in between these two values ($n_m < n_1$ or $n_m > n_2$). From Eqs. 1, 2, 3 the sign of J_1 is determined by the value of Δ at the Brewster angle, i.e. Δ can be +90 deg or -90 deg at φ_B. Note that the assumption $\Delta = +90$ deg at φ_B (where $\mathrm{Re}(r_p/r_s)$=0) is not strictly true. For incident light traveling through the lower refractive index media ($n_1 < n_2$), a transition from 0 to 180 deg around the Brewster angle, $\Delta = 90$ deg at φ_B, indicates a positive J_1; whilst J_1 is negative when a transition from 0 to -180 deg is measured ($\Delta = 90$ deg at φ_B). Whereas an opposite behavior is expected for incident and reflected light traveling through the higher refractive index media.

We could extract the value of J_1 from Eqs. 1 and 2 within an experimental error of ± 0.015 nm. For each experimental system several experiments have been carried out including changing conditions (alignment of the beam, freshly filtered solvent, cleaning, etc.). We have never seen a sign change for J_1 at a given interface.

The effect of the presence of contaminations on our measurements was also checked. When the interface was not accurately cleaned or when the active vibration table was not operative, the presence of dust particles or other undesirable substances or vibrations resulted in significant noises in Ψ and Δ. We compared the measured ellipsometric angles Ψ and Δ for the air/water interface measured in a commercial imaging ellipsometer (EP^3-SW, Nanofilm, Germany) and in our set-up [35]. The cell containing water in the commercial ellipsometer was also isolated by external vibration being the apparatus placed on top of an active vibration isolation table (Halcyonics, Germany). Dust and impurities could be visualized by the imaging ellipsometer by Brewster angle microscopy with spatial resolution of 1 micrometer. It was observed that impurities, which floated at the surface, did not organize homogeneously such in a surfactant monolayer. The ellipsometric signal was affected only when those micron-size impurities passed through the beam spot on the interface. Only for these measurements Ψ and Δ showed significant noises, whilst for the rest of the ellipsometric scan the change of Ψ and Δ with the angle of incidence remained smooth.

In Fig. 1 we compared the data obtained by the imaging ellipsometer and our set-up when the surface of water was accurately cleaned. The ellipsometric angles obtained by a commercial ellipsometer displayed some noise in particular close to the Brewster angle, where the sensitivity on the interfacial profile is maximum. The accuracy of data seems to drop for $\tan(\Psi) < 0.003$. This limit in data's accuracy can be ascribed either to not a robust fit of the polarizer and analyzer scans or to the internal vibrations produced by the apparatus. In fact, some internal coupling between the mechanical components of the commercial ellipsometer and the liquid cell could not be prevented.
In our experiments, optimizing the cleaning procedure, isolation from internal and external perturbations and having implemented a robust fitting procedure we could measure accurately Ψ and Δ with a negligible noise and with small error bars. Thus, the smooth profiles of Ψ and Δ as functions of the incident angle can be regarded as a fingerprint of the negligible contribution of interfacial impurities and vibrations to the measured signal.
For aqueous interfaces, we performed our measurements using also a cylindrical glass cell closed to the atmosphere during the experiments in order to avoid any effect of external pollution. Finally, for the latter interfaces we performed ellipsometric scans from both sides of the surface.

3 Results and Discussion

Fig. 2 shows ellipsometric data and fits for air/formic acid (A/F), air/decane (A/DE), air/dodecane (A/DD) and air/nmp (A/N). The sharp transition of Δ and the deep minimum in $\tan(\Psi)$ at the Brewster angle indicate small values of J_1. The accuracy of the applied nulling scheme is sufficient to resolve such small deviations from a step profile of the refractive index. Δ switches from 0 deg to 180 deg in those interface corresponding to a positive value of J_1. It is worth noting that the value of $\bar{\rho} = \tan(\Psi)\sin\Delta$ can be extracted accurately from our data, and Δ at the Brewster angle for the data reported in Fig. 2 is +90 deg.

Fig. 3 displays ellipsometric data and fits for water/dodecane (W/DD), air/water (A/W), and air/hydrazine monohydrate (A/H). For these interfaces differences in the depth of $\tan(\Psi)$

and the slope of Δ are even more significant than in Fig. 2. Moreover Δ for these interfaces switched from 0 to -180 deg corresponding to a value of $J_1 \leq 0$. For A/H interface, the transition in Δ is almost perfectly step-like and J_1 vanishes. Thus, on the contrary of the previous data, Δ at the Brewster angle is equal to -90 deg and the corresponding ellipticity $\bar{\rho}$ is negative. We can compare our result for air/water $\bar{\rho} \approx -10^{-3}$ with the predicted $+0.67\times10^{-3}$ or with the experimental $+0.4\times10^{-3}$ literature data reported by Meunier [11] and notice that values are of the same order of magnitude but of different sign.

To further prove the unexpected $J_1 < 0$ for A/W and W/DD interfaces, we performed ellipsometric scans with the incident light traveling through the higher refractive index media, i.e. water in the case of water/air (W/A) and dodecane for dodecane/water (DD/W). Ellipsometric scans shown in Fig. 4 confirm the unexpected behavior for the aqueous interfaces investigated here, the values of J_1 being really close to those obtained for A/W and W/DD.

Table 1 lists the fit parameters of the investigated liquid interfaces. The refractive index values of the macroscopic phases are in reasonable agreement with literature data. The ratio n_1/n_2 determines the location of the Brewster angle and a small adjustment inaccuracy shows up in this ratio. The first two columns show the refractive index of the bulk phases, which are in good agreement with literature values. The third column gives the fitting parameter J_1.
The latter values are the main results of this work.
Now, we will compare our experimental results with some theoretical predictions.

3.1 Comparison 1: couple mode theory for surface roughness

Firstly, we consider the interfacial profile in terms of surface roughness due to thermally excited capillary waves. Meunier described the surface roughness contribution to the ellipsometric signal in terms of the ellipsometric parameter η=-J_1 calculated in the approximation of independent capillary wave modes and considering mode coupling [11]. The interfacial roughness is described in terms of vertical displacement ζ_q of mode of wave vector q, and the corresponding ellipsometric parameter is given by:

$$J_1^R = \frac{3}{2}\frac{(n_1^2 - n_2^2)^2}{n_1^2 + n_2^2}\sum_q q\left\langle \zeta_q^2 \right\rangle, \tag{4}$$

The result of the summation of the last term in Eq. 4 is also reported by Day and Bain who expressed this roughness contribution to ellipticity $\bar{\rho}$ [27]. Here, the corresponding first order invariant term J_1^{CM} is given by:

$$J_1^{CM} = \frac{3}{2}\frac{(n_1^2 - n_2^2)^2}{n_1^2 + n_2^2}\sqrt{\frac{\pi k_B T}{6\gamma}}, \tag{5}$$

where k_BT is the thermal energy and γ is the interfacial tension. We calculated J_1^{CM} and we reported the values in Tab. 1. Theoretical predictions are in a good agreement with the experimental results for the data displayed in Fig. 2. However the predicted J_1^{CM} is always non-negative and this theory can not describe the experimental J_1 for the data displayed in Figs. 3 and 4.

3.2 Comparison 2: intrinsic structure theory

Here, we compare our results with the intrinsic structure theory. From Van der Waals theory, the profile of the density ρ across the interface can be described as an hyperbolic tangent

function [7]. Lekner calculated the exact expressions for the first and second order invariants for several profiles of the dielectric function ϵ_m=n_m^2 including the hyperbolic tangent one:

$$n_m^2(z) = \frac{1}{2}(n_1^2 + n_2^2) - \frac{1}{2}(n_1^2 - n_2^2)\tanh(z/2d). \tag{6}$$

In this case, the first order invariant is given by:

$$J_1^{HT}/d = (n_1^2 - n_2^2)\ln\frac{n_1^2}{n_1^2}, \tag{7}$$

where d is the interfacial width. For the estimation of d we used the same expression given by Day and Bain: $d^2 = \frac{k_b T}{4\pi\gamma}\ln\left(\frac{2\gamma\lambda^2}{3\pi k_B T}\right)$ (=0.25-0.41 nm) to remain consistent with the couple mode theory used in the first comparison [27]. The comparison of the theoretical J_1^{HT} with the experimental is shown in Tab. 1. Also in this case the theory predicts non-negative values and the difference between theory and experiment in this case is larger than in the couple mode theory for surface roughness. Note that the intrinsic profiles which describe the transition in pure liquid interface (also e.g. error function profile) predict non-negative J_1.

3.3 Dielectric profile and cohesive energy

At this point, it seems clear that dielectric profile measured by ellipsometry in our experiments can not be described by surface roughness and/or density profile.
In fact, we believe that a significant contribution of hydrophobicity, hydrogen bonds and dispersion forces (interactions between molecules at the interface) to the dielectric property of the interface must be taken into account. Day and Bain, to account for hydrophobicity, suggested a dependency with refractive index and surface tension [27]. We consider instead a parameter such a surface tension scaled with the molecular size. The latter parameter represents the cohesive energy and it is called Gordon parameter $G = \gamma V_m^{-1/3}$. This parameter is a measure of the cohesiveness of liquids and it was successfully used to understand micellization in different solvents [37]. Thus, the Gordon parameter can describe hydrophobic interactions of a liquid with other molecules including vapor/liquid interfaces.

Here, we will use the difference between the Gordon parameters of the two macroscopic phases $\delta G = G_{water} - G_{oil}$ for the oil-water interface and $\delta G = G_2$ for liquid-air interfaces (G_{air}=0, by definition).

The experimental J_1, displayed in Fig. 5, show a good correlation with δG suggesting that the interfacial profile probed by ellipsometry is strongly dependent on the cohesive interaction.

At this point some questions arise. Do the J_1-values manifest changes in nature and strength of interactions from non-associative liquids (low cohesive energy) to associative ones (high cohesive energy) [24], in which hydrogen bonds play a fundamental role in the interaction with the second media? Furthermore, are the changes of the sign of J_1 pointing to changes in the interfacial profile as predicted for polar liquids in contact with non-polar media? Moreover, what is the information given by $J_1 < 0$ for the refractive index of the interfacial layer? Is this latter value greater than n_2 or smaller than n_1?
For oil/water interfaces, Day and Bain [27] discussed that a depleted layer $n_m = 1 <$min(n_1,n_2) with a thickness of ca 0.03 nm exists at water-oil interfaces. We believe that the value of 0.03 nm obtained by Day and Bain can not describe the interfacial profile, being one order of magnitude lower than the surface roughness. It is clear also that in our case, for air/liquid interfaces, a negative value J_1 can not be interpreted in terms of layer with a refractive index smaller than air, being this result physically meaningless, i.e. $n_m < n_1$=1.

3.4 Uniform layer model and anisotropy

We could discuss our findings also from a different viewpoint. In fact, we can compare our data assuming either a uniform layer model or anisotropy. Both approximations can explain negative

J_1 values.
In the first case, we fitted our ellipsometric scans within a stratified homogeneous layer model [9], where the thickness t and the refractive index n_m of the layer are the unknow parameters. We decided to fix the thickness t and fit n_m and we chose $t = 0.6$ nm for all the interfaces studied. The latter value is an average between the interfacial width d calculated from the couple mode theory and the $10\% - 90\%$ thickness ($= 4.394d$) [12]. The results of the fits are shown in Fig. 6a. Note that a single solution for n_m corresponds to the case $J_1 > 0$, whereas two distinct solutions can be found for $J_1 < 0$.
For the interfaces at low cohesive energy δG, values of n_m are in between the bulk values as expected, whilst for high δG values n_m is either lower than $\min(n_1, n_2)$ or higher than $\max(n_1, n_2)$. These different solutions for n_m correspond also to a different nature of interactions between the bulk phases through the interphase. Knowing the interfacial refractive index n_m, we calculated the frequency-dependent Hamaker constant $A_{1m2}(\lambda) = A_\lambda$ which describes the dispersion interaction between media 1 and 2 through media m. A_λ can be expressed by [3]:

$$A_\lambda \sim \frac{3h\nu_e}{8\sqrt{2}} \frac{(n_1^2 - n_m^2)(n_2^2 - n_m^2)}{\sqrt{n_1^2 + n_m^2}\sqrt{n_2^2 + n_m^2}(\sqrt{n_1^2 + n_m^2} + \sqrt{n_2^2 + n_m^2})}, \tag{8}$$

where $\nu_e \sim 3.0\, 10^{15} \mathrm{s}^{-1}$ is the main electronic absorption frequency. Results of the the calculation of A_λ are shown in Fig. 6b. The calculated frequency-dependent Hamaker constant A_λ follows a trend opposite to J_1 (Fig. 5) changing from a negative value to a positive one with increasing δG. In other words a repulsive interaction across an interfacial zone is calculated at low δG whereas at high δG the interaction forces between molecules at the interface turn attractive.
However, in this uniform layer approximation, it is worth noting that physically acceptable n_m (> 1) values for aqueous interfaces seem overestimated, being $n_m \approx 1.4$.
In a better approximation, anisotropy of the interfacial layer can be assumed since orientation of molecules at the interface is expected for high values of δG. To account for anisotropy, the definition of J_1 changes [10]:

$$J_1 = \int_{-\infty}^{+\infty} \left(n_1^2 + n_2^2 - \frac{n_1^2 n_2^2}{n_\perp^2} - n_\parallel^2 \right) \, \mathrm{d}z, \tag{9}$$

where $n_\perp(z)$ and $n_\parallel(z)$ are the refractive indexes profiles perpendicular and parallel to the interface. To simplify the calculation of Eq. 9 we assumed also uniform layer profile, as suggested by Beaglehole for ice/water interfaces [19]. The unknown interfacial parameters in this case are $n_\parallel$, $n_\perp$ and the interfacial thickness. We fixed the $10\% - 90\%$ thickness $t = 4.394d$ and discuss the $n_\parallel$ and $n_\perp$ just for aqueous interfaces. If we assumed a ordered layer on the interfacial plane such ice $n_\parallel$=1.309, the corresponding $n_\perp$ are: 1.245 (air/hydrazine monohydrate), 1.303 (dodecane-water) and 1.23 (air-water). For air-liquid interfaces, the latter values are in well agreement with an averaged refractive in between the bulk values and for dodecane-water interface $n_\perp \approx n_\parallel$.

From all these considerations, we can not say whether there is a depleted layer ($n_m = 1$) at the oil/water interface or not, but, in a good approximation, the effect of partial ordering of molecules at the air/water interface can explain negative J_1 values. Our results showed high accuracy and reproducibility and over all the measurements performed never was measured a significantly different profile for A-W interface. We pointed out the correlation between the dielectric profile at the interface and the cohesive energy δG. At low δG the interfacial profile results could be explained by surface roughness. Whereas, at high δG the interfacial profile can be considered strongly affected by charge accumulation, hydrogen bonds and attractive interactions between molecules sitting in the interfacial region. In the case of A/H interface, these two contributions are approximately balanced resulting in an almost step-like profile. This step-like profile can be the result of specific interactions between hydrazine and water. In fact, H-bonding between water hydrogens and nitrogen atoms causes stiffening of hydrazine. Thus, the hydrazine-water complex (hydrazine monohydrate) rests flat and stiff at the interface exposing the hydrazine part to air.

A quantitative interpretation of the experimental results, however, depends on the model and on the assumptions made. From this viewpoint, our results can be compared with the theoretical prediction and experimental observations of partial ordering of water molecules at the interface due to hydrogen-bonding network [18].

Conclusions

In conclusion, a systematic study of different interfaces show surprisingly results when the cohesive energy (quantified by δG) is increased. The interfacial profiles measured by high resolution ellipsometry are compared with several theories and experiments and discussed also in terms of interactions in the interfacial plane such as hydrogen bonding and dispersive interactions. For aqueous interfaces (at high values of δG), negative J_1 values can be interpreted considering ordering of molecules due to hydrogen-bonding network.

Acknowlegdements

A.S thanks Dominique Langevin for the support, Hubert Motschmann and Markus Antonietti for interesting discussions, and Liliane Leger for lending the Nanofilm ellipsometer. Financial support of the Max Planck Society and University of Palermo is gratefully acknowledged.

References

1. T. P. Russell, J. Bae, *Polymers, liquids and colloids in electric fields* Interfacial Instabilities, Orientation and Phase Transitions, Y. Tsori, U. Steiner (editors), (World Scientific Publishing Co. Pte. Ltd. , 2009) 113-148
2. K. Tauer, S. Kozempel, G. Rother J. Colloid and Interface Sci., **312** ,432-438 (2007)
3. J. Israelachvili, *Intermolecular and Surface Forces* (Academic Press, Amsterdam, 1991)
4. R. Sigel, G. Strobl, J. Chem. Phys., **112**, 1029-1039 (2000)
5. E. W. Lang, H. D. Lüdemann, Angewandte Chemie, Int. Ed., **21**, 315-388 (1982)
6. H. Lamb, *Hydrodynamics* (Dover, New York, 1945)
7. D. Beysens, M. Robert, J. Chem. Phys., **87**, 3056-3061 (1987)
8. D. Langevin, *Light Scattering by Liquid Surfaces and Complementary Techniques* (Marcel Dekker, New York, 1992)
9. R.M.A. Azzam, N.M. Bazhara, *Ellipsometry and polarized light* (Elsevier, Amsterdam, 1977)
10. J. Lekner, *Theory of Reflection*(Martinus Nijhoff Publishers, Dordrecht, 1987)
11. J. Meunier, J. de Physique, France, **48**, 1819-1831 (1987)
12. D. Beaglehole, J. Physiol. Suppl., Paris, **44**, C10, (1983)
13. D. Beaglehole, Phys. Rev. Lett., **58**, 1434-1436 (1987)
14. T.R. Jensen, M.O. Jensen,N. Reitzel, K. Balashev,G.H. Peters, K. Kjaer, T. Bjornholm, Phys. Rev. Lett., **90**, 086101 (2003)
15. M. Mezger, S. Schoder, H. Reichert, H. Schroder, J. Okasinski, V. Honkimaki, J. Ralston, J. Bilgram, R. Roth, H. Dosch, J. Chem. Phys., **128**, 244705 (2008)
16. K. Lum, D. Chandler, J.D. Weeks, J. Phys. Chem. B **103**, 4570-4577 (1999)
17. N.T. Southall, K.A. Dill, J. Phys. Chem. B **104**, 1326-1331 (2000)
18. Y.R. Shen, V. Ostroverkhov, Chem. Rev. **106**, 1140-1154 (2006)
19. D. Beaglehole, P. Wilson, J. Phys. Chem. **97**, 11053-11055 (1993)
20. W.F. Murphy, J. Phys. Chem. **67**, 5877-5882 (1977)
21. Y.H. Zhang, S.E. Feller, B.R. Brooks, R.W. Pastor, J. Phys. Chem. **103**, 10252-10266 (1995)
22. G.C. Lie, S. Grigoras, L.X. Dang, D.Y. Yang, A.D. McLean, J. Phys. Chem. **99**, 3933-3937 (1993)
23. K.N. Kudin, R. Car, J. Am. Chem. Soc. **130**, 3915-3919 (2008)
24. U. Raviv, P. Laurat, J. Klein, Nature, **413**, 51 (2001)
25. T.M. Truskett, P.G. Debenedetti, S. Torquato, J. Chem. Phys., **114**, 2401 (2001)

26. D. Derks, D.G.A.L. Aarts, D. Bonn, H.N.W. Lekkerkerker, A. Imhof, Phys. Rev. Lett. **92**, 038301 (2006)
27. J.P.R Day, C.D. Bain, Phys. Rev. E, **76**, 041601 (2007)
28. S. Mora, J. Daillant, K. Mecke, D. Luzet, A. Braslau, M. Alba, B. Struth, Phys. Rev. Lett., **90**, 216101 (2003)
29. A. Stocco, G. Haseloff, A. Erbe, K. Tauer, R. Sigel, *submitted to Phys. Rev. E*
30. A. Erbe, K. Tauer, R. Sigel, Phys. Rev. E, **73**, 031406 (2006)
31. A. Erbe, K. Tauer, R. Sigel, Langmuir, **23**, 452-459 (2007)
32. A. Erbe, R. Sigel, Eur. Phys. J. E, **22**, 303-309 (2007)
33. A. Erbe, K. Tauer, R. Sigel, Langmuir, **25**, 2703-2710 (2009)
34. A. Erbe, R. Sigel, Appl. Opt., **12**, 2161-2170, (2008)
35. We represented our data using the convention adopted by Lekner, i.e. $r_p = r_s$ at normal incidence.
36. T.E. Daubert, R.P. Danner, H.M Sibul, C.C. Stebbins, *Physical and thermodynamic properties of pure chemicals: data compilation* (Taylor and Francis, Washington DC, 1998)
37. T.L. Greaves, A. Weerawardena, C.Fong, C.J. Drummond, J. Phys. Chem. B, **111**, 4082-4088 (2007)
38. F. Evans, H. Wennerstrom, *The Colloidal Domain* (Wiley, New York, 1999)

	n_1	n_2	J_1 (nm)	γ ($\mathrm{mNm^{-1}}$)	J_1^{CM} (nm)	J_1^{HT} (nm)	V_{mol} ($\mathrm{m^3Kmol^{-1}}$)
air/formic ac.	1	1.372	0.057	37.1	0.097	0.192	0.038
air/decane	1	1.407	0.110	23.4	0.145	0.284	0.196
air/dodecane	1	1.418	0.143	24.9	0.149	0.293	0.229
air/NMP	1	1.464	0.116	42.2	0.139	0.281	0.097
air/hydrazine m.	1	1.416	0.000	65.6	0.090	0.184	0.032
water/dodecane	1.335	1.418	-0.039	52.1	0.004	0.008	-
air/water	1	1.335	-0.122	72.8	0.056	0.113	0.018
dodecane/water	1.418	1.336	-0.032	52.1	0.004	0.008	-
water/air	1.330	1	-0.119	72.8	0.056	0.113	0.018

Table 1. Refractive indexes n_1 and n_2 used in the models, experimental fitting parameter J_1, interfacial tension γ [36], predicted first order invariant from the couple mode theory J_1^{CM} (calculated), predicted first order invariant from an hyperbolic function profile J_1^{HT} (calculated) and molar volume V_{mol} [36].

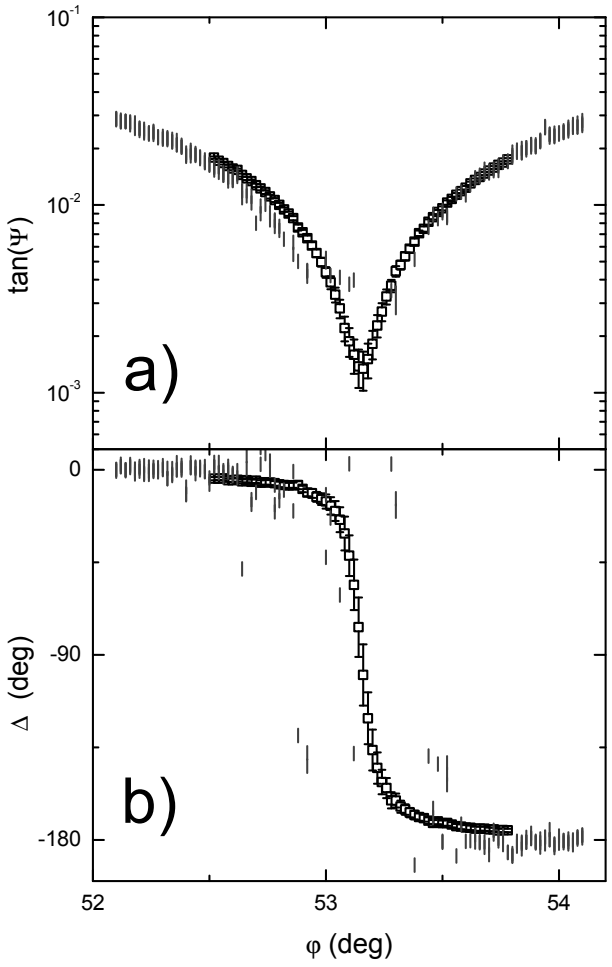

Fig. 1. Comparison between $\tan(\Psi)$ (a) and Δ (b) for air/water interfaces measured by means of a commercial ellipsometer (|) (Nanofilm, Germany) and by the home built apparatus (□) described in Ref. [29].

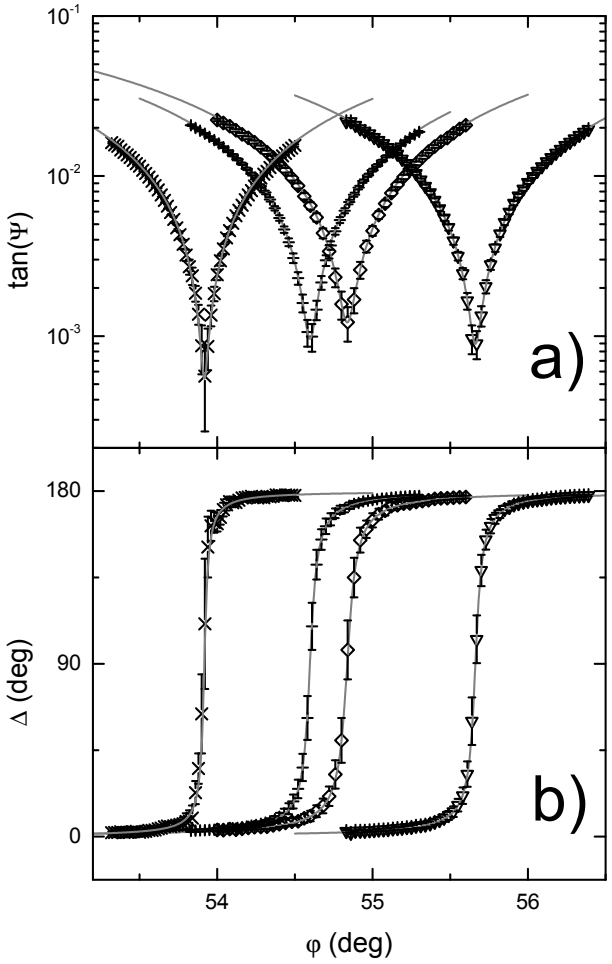

Fig. 2. tan(Ψ) (a) and Δ (b) scans at the air/formic acid (X), air/decane (+), air/dodecane ($\diamond$) and air/nmp ($\triangledown$) interface. Solid lines are the fits corresponding to the J_1 reported in the Table 1.

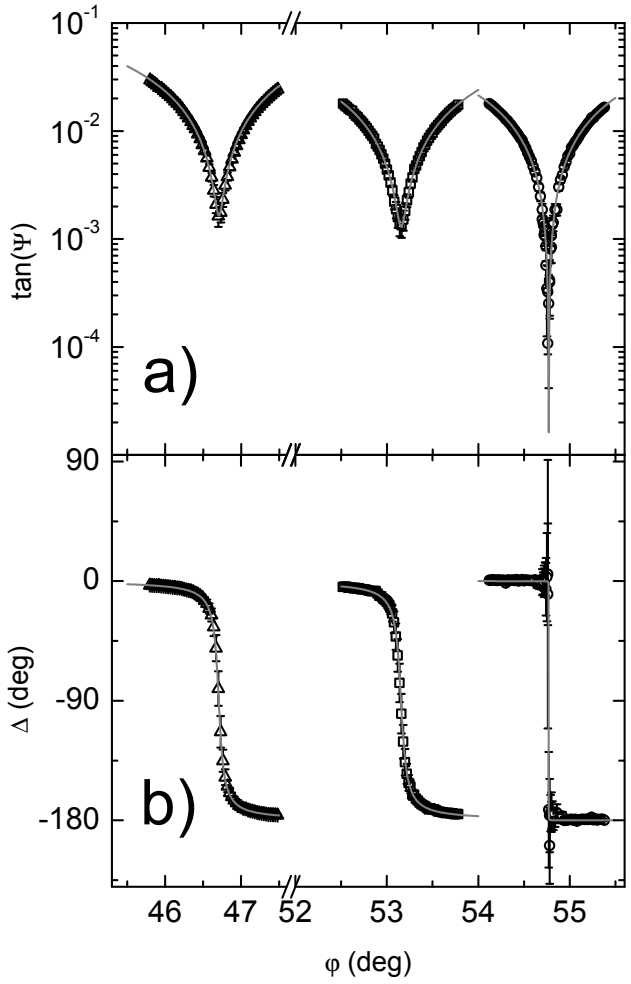

Fig. 3. tan(Ψ) (a) and Δ (b) scans at the water/dodecane ($\triangle$), air/water ($\square$), and air/hydrazine monohydrate ($\circ$) interface. Solid lines are the fits corresponding to the J_1 reported in the Table 1.

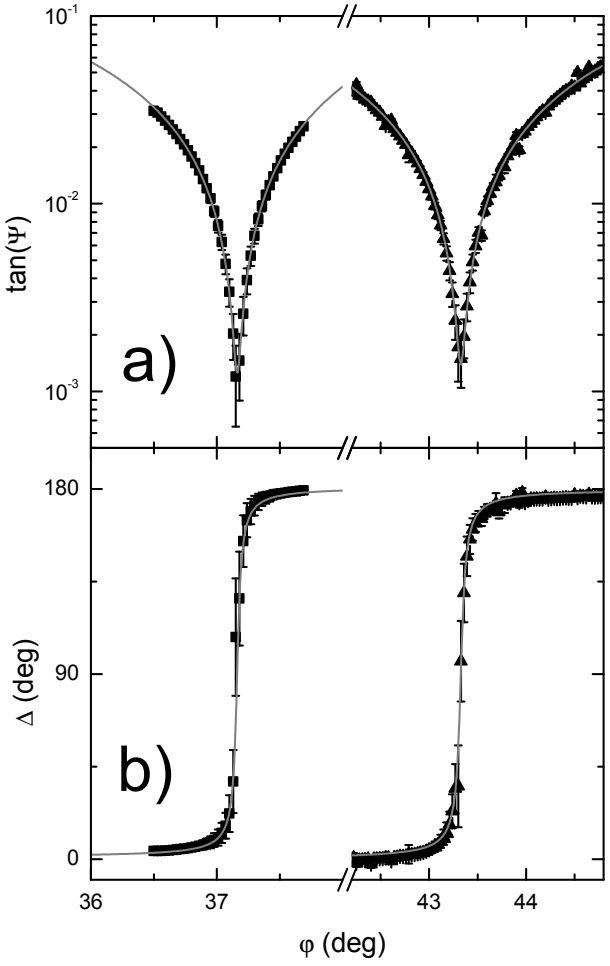

Fig. 4. tan(Ψ) (a) and Δ (b) scans at the water/air (■), dodecane/water (▲) interface. Solid lines are the fits corresponding to the J_1 reported in the Table 1.

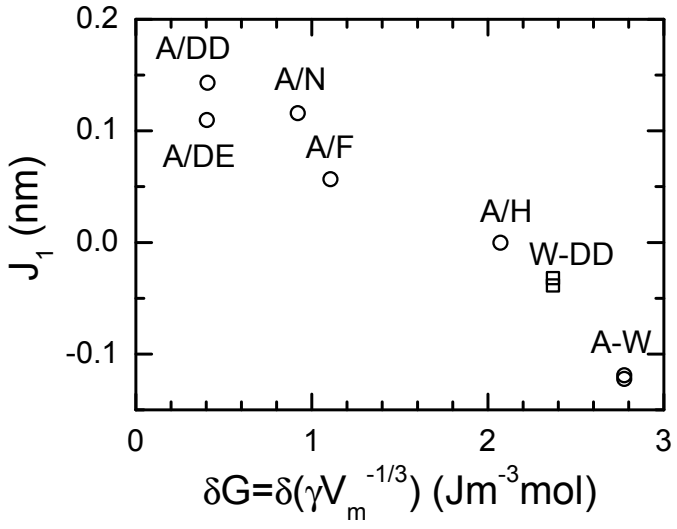

Fig. 5. Experimental value of J_1 (first order invariant term) based on the Perturbation theory plotted versus the difference of Gordon Parameter between the two fluid phases.

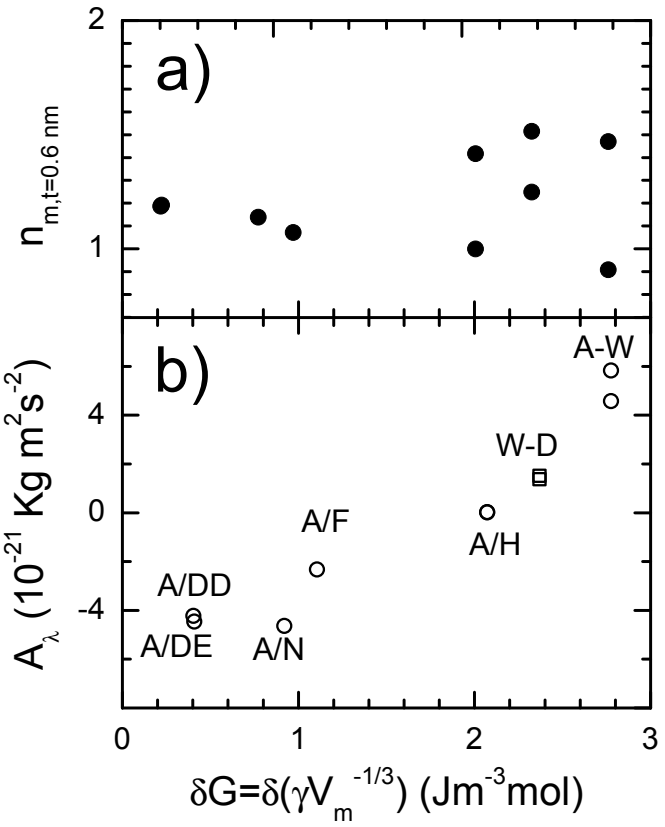

Fig. 6. Refractive index n_m of the uniform layer of thickness $t = 0.6$ nm (a) and Hamaker constant A_λ (b) plotted versus the difference of Gordon Parameter.